

## MICROSTRUCTURE OF SELECTED METAMORPHIC ROCK TYPES – APPLICATION OF PETROGRAPHIC IMAGE ANALYSIS

Šárka ŠACHLOVÁ<sup>1,2)\*</sup>, Vladimír SCHENK<sup>2)</sup> and Zdeňka SCHENKOVÁ<sup>2)</sup>

<sup>1)</sup> *Institute of Geochemistry, Mineralogy and Mineral Resources, Faculty of Science, Charles University in Prague, Albertov 6, 128 43 Prague 2, Czech Republic*

<sup>2)</sup> *Institute of Rock Structure and Mechanics, Academy of Sciences of the Czech Republic, v.v.i., V Holešovičkách 41, 182 09 Prague, Czech Republic*

\*Corresponding author's e-mail: lukschova@seznam.cz

(Received August 2010, accepted November 2010)

### ABSTRACT

Microscopic techniques, such as polarising microscopy and scanning electron microscopy with energy dispersive spectrometer (SEM/EDS), were used in combination with petrographic image analysis with the aim of a quantitative determination of the mineral composition, rock microstructure, and degree of metamorphism of selected quartz-rich metamorphic rock types. Sampled orthogneiss rock types are mainly composed of feldspar, quartz, biotite, and amphibole. The grains are less isometric, elongated, having smooth boundaries, and showing a weak preferential orientation. The deformation and recrystallization characteristics of quartz indicate high-temperature recrystallization (the grain boundary migration recrystallization mechanism). Schist and phyllite rock types are preferentially very-fine to fine-grained, showing a strong shape preferred orientation. Their sedimentary origin was indicated by the presence of graphite. The deformation and recrystallization characteristics of the quartz indicate low temperature conditions of their metamorphism.

**KEYWORDS:** metamorphic rock, texture, structure, microscopy, kinematic indicators

---

### INTRODUCTION

Metamorphic rock types are classified as "...originally either igneous or sedimentary, but their character has been changed by processes operating below the surface of the Earth. The constituent minerals of the rocks may be changed, or the shapes, sizes and mutual spatial relationship of the crystals may change. There are a variety of processes involved, and they are collectively described by the term metamorphism." (Mason, 1990). Metamorphic rocks are classified according to their source rock type, structure, microstructure and mineral composition (see more in the principles of the IUGS scheme for Classification of Igneous Rocks and the pending IUGS classification scheme for metamorphic rocks; Le Maitre et al., 1989; Robertson, 1999). Mineral composition is a parameter that reflects the proportions of the individual minerals within the rock. Rock structure represents all of the macroscopically visible characteristics such as foliation, lineation, folding, and faulting (Spry, 1969; McPhie et al., 1993; Bucher and Frey, 1994). Microstructure comprises the geometrical parameters of rock-forming minerals such as grain size, grain shape, and spatial arrangement of minerals visible in micro-scale (Vernon, 2004). Most of the parameters mentioned above are commonly described qualitatively, employing polarising microscopy.

The combination of polarising microscopy along with image analysis makes it possible to determine the mineral composition, as well as the microstructural parameters quantitatively (e.g., Heilbronner, 2000; Trčková et al., 2008), which increases the objectivity and accuracy of the microscopic description. Fully-automatic image analysis distinguishes objects from the background according to their colour differences (e.g., Ehrlich et al., 1991). During semi-automatic image analysis, objects are captured by the operator (e.g., Siegesmund et al., 1994; Příkryl, 2006).

This paper aims to: (1) quantify the mineral composition and microstructure (grain size, and grain shape) of variol quartz-rich metamorphic rock types; as well as (2) apply these parameters in the interpretation of the tectonic history of the investigated rocks. The metamorphic conditions of the investigated samples were estimated based on the mineral assemblages, quartz deformation, and recrystallization characteristics. From the methodological point of view, the reliability of the application of petrographic image analysis has been verified.

### EXPERIMENTAL

#### SAMPLING

The samples were selected based on the following criteria: (1) quartz represents the principal

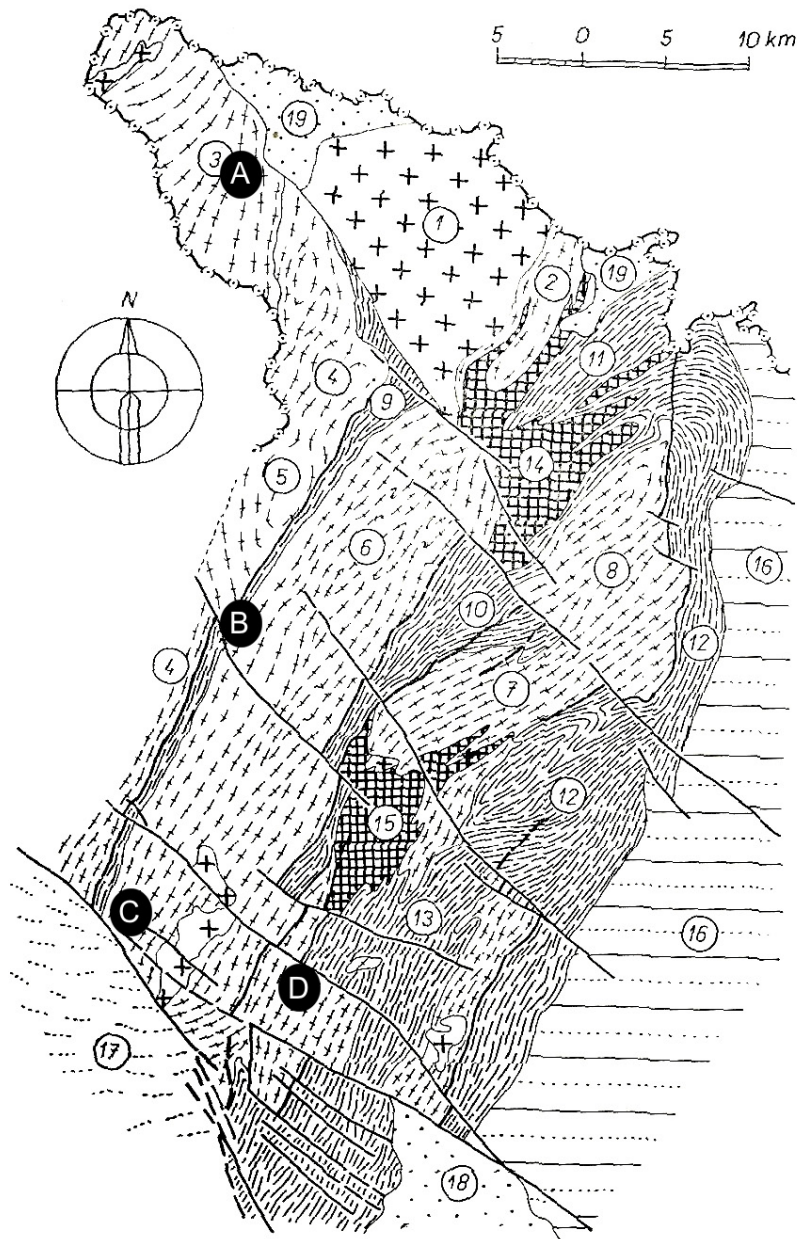


**Fig. 1** Schematic geologic map of NE part of Bohemian massif with the position of quarries (accepted from Svoboda et al., 1964, modified). A – 15.1, B – 18.1, C – 18.2, D – 18.3, 1-2 – Žulová complex and its surroundings, 3 – Orlica-Snieznik dome, 4 – Staré Město belt, 5 – Velké Vrbno unit, 6 – Keprník dome, 7-8- Desná dome, 9 – Branná unit, 10 – Červená hora unit, 11 – Rejvíz area, 12-13 Hrabíšín area, 14 – Jeseník amphibolite complex, 15 – Sobotín amphibolite complex, 16 – Andělská hora area, 17 – Zábřeh area, 18 – hornomoravský úval, 19 – Quaternary sediments.

compound; (2) quartz shows different deformation and recrystallization characteristics; (3) minerals indicating a degree of metamorphism are included.

The rock types were sampled from quarries located in the Czech Republic (Orlica-Snieznik dome

and Silesian domain, see Figure 1), as well as in Sweden (Svecofennian province, see Figure 2). Only one sample was taken from a natural outcrop (Sample No. 15-1) previously investigated as a potential area for a new quarry (Puda and Urbánek, 1972).

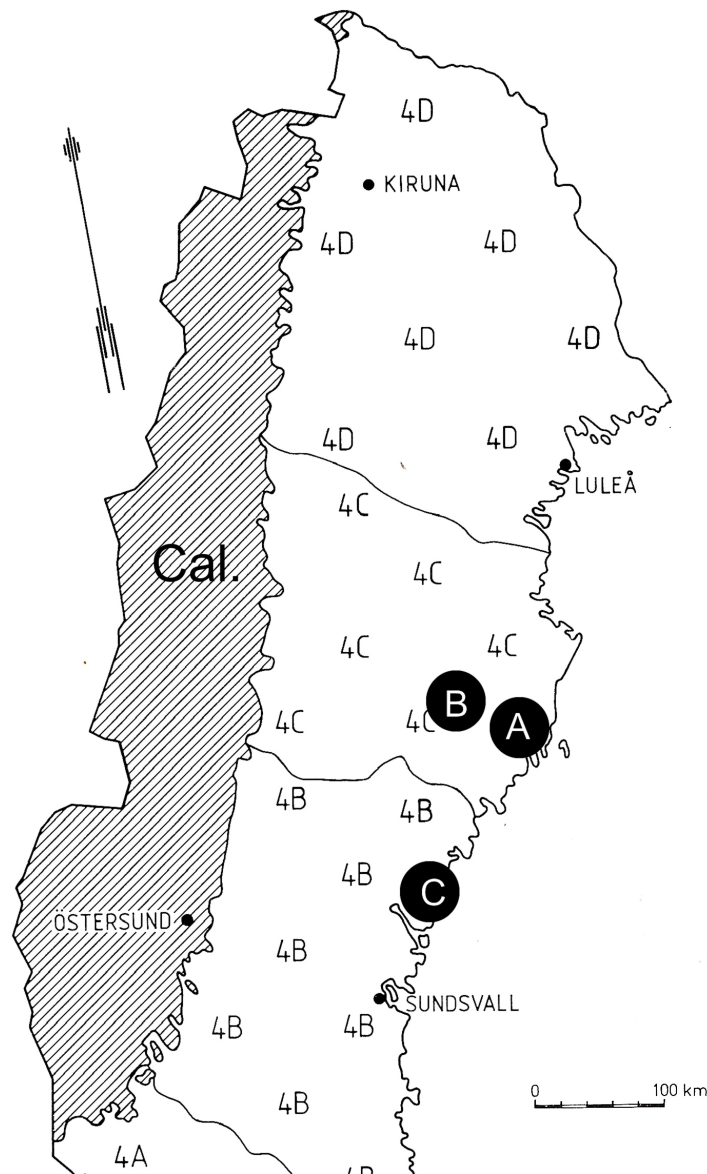


**Fig. 2** Schematic geologic map of Northern part of Svecofennian province (Sweden) with the position of quarries (accepted from Lundqvist, 1979; Rutland et al., 2001; modified). A – 04-1, B – 07-2, C – 11-1, 4 – Svecofennian province ( $\approx$  Svecokarelian orogenic belt) including post-orogenic and anorogenic complexes, 4A – Götaland and Svealand, 4B – Southern Norrland, 4C – Västerbotten Country and southernmost Norrbotten Country, 4D – Norrbotten Country, Cal. – Caledonides.

The Orlica-Snieznik dome and the Silesian domain form the NE portion of the Bohemian Massif. The Orlica-Snieznik dome is generally composed of medium to high-grade gneisses (“Snieznik gneiss”), schist, and granitoids of Cambro-Ordovician age (480 - 520 MA; Don et al., 1990; Oliver et al., 1993; in Štípská et al., 2001). The high-grade gneisses contain boudines of eclogites and granulites, indicating metamorphic conditions of 18 - 25 kbar and 800 - 900 °C (Kryza and Pin, 2010). “Snieznik gneiss”

(Sample No. 15-1, sampled from natural outcrop close to the Račí potok) could be macroscopically described as a medium to coarse-grained, grey to red granoblastic gneiss with a weak foliation composed of K-feldspar, quartz, albite, apatite, titanite, and hornblende (Ondra and Potměšil, 1965).

The Silesian domain (subdivided into the Staré Město belt, Velké Vrbo unit, Desná dome, and Keprník dome regional geological units, see Figure 1) is characterized by various metamorphic rocks

**Table 1** List of samples, including their geologic characterisations. (\*) - rock type indicated by previous investigation (Lundqvist et al., 1979; Šitavanc and Souček, 1986; Novák et al., 1988; Zimák and Novotný, 2000; Rutland et al., 2001; Štípská et al., 2001).

Sample No.	Quarry / outcrop	Geological unit	Area	Regional geological unit	Geological sub-unit	Rock type (*)
15-1	Račí údolí	Bohemian Massif	Lugicum	Orlica-Snieznik dome	Vilémovice area	orthogneiss
18-1	Branná	Bohemian Massif	Moravo-Silesian	Silesian	Branná area	phyllite
18-2	Bohutín-Zbová	Bohemian Massif	Moravo-Silesian	Silesian	Keprník dome	hybrid gneiss
18-3	Krásné u Šumperka	Bohemian Massif	Moravo-Silesian	Silesian	Desná dome	schist
04-1	Stoningsberget (Umea)	Fennoscandia	Svecofennian province	Västerbotten Country		orthogneiss
07-2	Orrberget (Vannas)	Fennoscandia	Svecofennian province	Västerbotten Country		orthogneiss
11-1	Getberget	Fennoscandia	Svecofennian province	Southern Norrland		schist

including orthogneiss, paragneiss, schist, amphibolite, and mylonite. Its metamorphic history is comprised of Barrovian-type metamorphism (ranging from a chlorite zone in the east to a kyanite zone in the west) and by later HT-LP metamorphism (Štípská et al., 2001). The samples were taken near to villages of Branná (Sample No. 18-1), Bohutín (Sample No. 18-2), and Hraběšice (Sample No. 18-3).

The Svecofennian province comprises those Precambrian regions in which a significant portion of the bedrock was affected by Svecofennian folding and metamorphism, or was formed in close association with these orogenic events (1750 - 1900 Ma). The region was predominantly metamorphosed to greenschist and amphibolite facies (Lundqvist, 1979; Claesson and Lundqvist, 1995; Sandström et al., 2009). Three selected samples were taken from Southern Norrland (Sample No. 11-1) and Västerbotten province (Samples No. 04-1 and 07-2, see Table 1).

Metamorphic rocks are well known for their variable microstructure with respect to the degree of foliation. Two oriented samples were taken from each quarry (or outcrop): one perpendicular to the foliation (a), and one parallel to the foliation (b), with an aim to better characterise the samples.

#### POLARISING MICROSCOPY

The polarising microscopy served for the basic description of the thin sections, including the (1) description of the rock microstructure, and (2)

identification of the primary minerals, as well as their alteration and deformation characteristics. A Leica DMLP polarising microscope (Optical Laboratory of the Institute of Geochemistry, Mineralogy, and Mineral Resources) was employed. A series of microphotographs were taken (using an Olympus digital camera), which later served for the petrographic image analysis.

#### SEM/EDS

Scanning electron microscopy with energy diffraction analysis (SEM/EDS analysis) was conducted at the Laboratory of Electron Microscopy and Microanalysis (Laboratories of the Geological Institutes, Faculty of Science, Charles University in Prague). The measurements were carried out using a Cambridge Cam Scan S4 with an energy dispersive analytical system (Oxford Instruments LINK ISIS 300) under the following conditions: beam current of 3 nA, and an accelerating voltage of 20 kV. A 53 Minerals Standard set #02753-AB (SPI Supplies) was used for the routine quantitative calibration. The SEM/EDS analysis facilitated identification of the mineral composition of very fine grained minerals.

#### PETROGRAPHIC IMAGE ANALYSIS

The semi-automatic image analysis consisted of the following steps: (1) image acquisition, which refers to the selection of a measured area within the thin sections (the size of the analysed area is controlled by the average grain size; at least 400

**Table 2** Parameters measured using petrographic image analysis. Q - quartz, F - feldspar, M - mica. \* - definitions accepted from SigmaScanPro 5 software (Systat Software Inc., 2010).

Parameter	Unit	Definition
Area (A)	pixels, mm <sup>2</sup>	* Area reports the area for the selected object.
Mineral composition	%	Mineral composition reflects the proportions of individual minerals in the rock calculated as total area of individual mineral divided by total area of the rock (e.g., mineral composition = Q (40%), F (40%), M (20%); $Q = \sum A_Q / \sum A_{TOT}$ ; $F = \sum A_F / \sum A_{TOT}$ ; $M = \sum A_M / \sum A_{TOT}$ ).
Equivalent diameter	pixels, mm	Equivalent diameter is calculated as a diameter of circle, which has the same area (A) as measured object - $D_{equiv} = (4 \times A / \pi)^{1/2}$ (Petruk, 1986)
Major axis length	pixels, mm	* Major axis of the object (defined by the two most distant points on the object) reports the length of the axis.
Minor axis length	pixels, mm	* Minor axis of the object (defined by the two most distant points on the object that creates a line perpendicular to the major axis) reports the length of the axis.
Major axis slope	-	* Major axis slope is defined as the slope of major axis of the object (defined by the two most distant points on the object).
Minor axis slope	-	* Minor axis slope is defined as the slope of minor axis of the object (defined by the two most distant points on the object that creates a line perpendicular to the major axis).
Shape preferred orientation	-	Shape preferred orientation of investigated samples indicates spatial arrangement of individual grains in respect to the horizontal axes of the thin sections. It is measured by the slope of major axis of individual grains, which means the angle between the major axis and horizontal axis of the digital images (e.g., Zhang <i>et al.</i> , 2002).
Perimeter (P)	pixels, mm	* The measurement account perimeter by approximating the vertical, horizontal and diagonal components of the object's true perimeter. The larger the object (in pixels), the more accurate the perimeter calculation will be.
Grain ellipticity	-	Grain ellipticity reflects the ratio between the minor and major axis lengths. Minor-to-major axis ratio close to 1 indicates isometric grains. Minor-to-major axis ratio close to 0 indicates elongated grains (Přikryl, 2006).
Shape factor (SF)	-	* Shape factor indicates circularity of investigated object (resp. grains). Ideal circle shows a shape parameter 1, objects with elongated or irregular shape show a shape factor close to 0 (Howarth & Rowlands, 1987). $SF = 4 \times \pi \times A / P^2$ .
Specific surface	mm/ mm <sup>2</sup>	Calculated from perimeter (P) divided by area (A) (e.g., del Amo & Perez, 2001).

grains are measured); (2) image digitising, which refers to the step in which selected area of the thin section is photo-documented using a digital camera; (3) image pre-processing, which includes the step in which the images are graphically modified, with the object to increase the contrast between the measured objects and the background by image analysis, as well as to prepare an accurate “map” of the minerals; (4) image measurement, where the image analysis software was employed and selected parameters (e.g.,

area) are measured; and (5) the data analysis. More details connected with petrographic image analysis can be studied elsewhere (e.g., Přikryl, 2006; Lukschová *et al.*, 2009).

The process of image analysis is semi-automatic. Thus, the difference between the objects measured, differences between objects and the background, as well as the objects' characterisation are controlled by the operator. The following parameters were evaluated using petrographic image analysis: area, major and

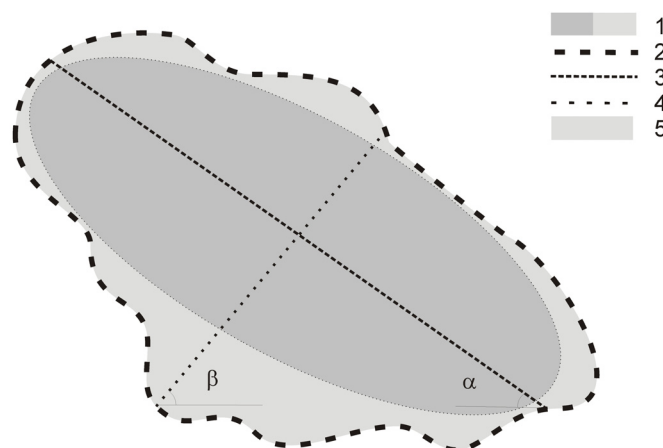


**Fig. 3** Parameters measured by petrographic image analysis. 1 – area, 2 – perimeter, 3 – major axis length, 4 – minor axis length, 5 – smoothness,  $\alpha$  – major axis slope,  $\beta$  – minor axis slope ( $\alpha + \beta = 90^\circ$ ).

**Table 3** Mineral composition of the investigated rock types (all values in vol.%). Q - quartz, F - feldspar (<sup>P</sup> - plagioclase > K-feldspar), M - mica (the primary mica mineral is indicated: <sup>msc</sup> - muscovite, <sup>bt</sup> - biotite, <sup>s</sup> - sericite, <sup>chl</sup> - chlorite), A - amphibole, C – calcite, NI - not identified by use of polarising microscopy, SEM/EDS - minerals analysed employing SEM/EDS method, n.a. - not analysed, b.d.l. - below definition limit (1.0 %).

Sample No.	Q	F	M	A	NI (SEM/EDS)	Accessory m. (SEM/EDS)	Tot.
04-1a	37.25	38.79 <sup>P</sup>	23.96 <sup>bt</sup>	n.a.	n.a.	apatite, titanite	100
04-1b	38.02	38.35 <sup>P</sup>	23.62 <sup>bt</sup>	n.a.	n.a.	apatite, titanite	100
07-2a	22.10	58.33 <sup>P</sup>	11.10 <sup>bt</sup>	8.48	n.a.	ilmenite, rutile, apatite, allanite	100
07-2b	21.28	68.62 <sup>P</sup>	3.82 <sup>bt</sup>	6.28	n.a.	ilmenite, rutile, apatite, allanite	100
15-1a	32.12	54.48 <sup>P</sup>	5.73 <sup>chl</sup>	7.68	n.a.	ilmenite, apatite, titanite	100
15-1b	34.54	51.18 <sup>P</sup>	6.33 <sup>chl</sup>	7.95	n.a.	ilmenite, apatite, titanite	100
18-1a	15.63	n.a.	16.16 <sup>bt,s</sup>	n.a.	68.21 (C, Q, F, M)	titanite, Fe-oxyhydroxides, organic matter	100
18-1b	17.45	n.a.	17.88 <sup>bt,s</sup>	n.a.	64.67 (C, Q, F, M)	titanite, Fe-oxyhydroxides, organic matter	100
18-2a	36.36	42.47	5.56 <sup>msc,bt</sup>	n.a.	15.62 (Q, F, M)	ilmenite, apatite, rutile	100
18-2b	37.89	43.44	4.69 <sup>msc,bt</sup>	n.a.	13.98 (Q, F, M)	ilmenite, apatite, rutile	100
11-1a	18.65	n.a.	14.53 <sup>msc,s</sup>	n.a.	66.82 (Q, F, M)	ilmenite, organic matter	100
11-1b	22.58	n.a.	17.90 <sup>msc,s</sup>	n.a.	59.52 (Q, F, M)	ilmenite, organic matter	100
18-3a	30.19	30.10	15.97 <sup>msc,bt</sup>	n.a.	23.73 (Q, F, M)	ilmenite, apatite	100
18-3b	34.14	30.36	14.97 <sup>msc,bt</sup>	n.a.	20.53 (Q, F, M)	ilmenite, apatite	100

**Table 4** Average values (Av.) and standard mean deviation (SMD) of equivalent diameter, shape factor (SF), grain ellipticity and specific surface.

Sample No.	Equivalent diameter		SF	G. ellipticity	Specific surface
	Av. (mm)	SMD	Av.	Av.	Av. (mm/mm <sup>2</sup> )
04-1a	0.24	0.14	0.60	0.57	27.23
04-1b	0.24	0.11	0.53	0.47	29.82
07-2a	0.33	0.20	0.56	0.57	20.52
07-2b	0.39	0.24	0.55	0.56	21.63
15-1a	0.28	0.17	0.59	0.60	27.85
15-1b	0.28	0.15	0.56	0.55	28.31
18-1a	0.02	0.00	0.66	0.73	170.19
18-1b	0.02	0.00	0.61	0.65	171.79
18-2a	0.05	0.01	0.61	0.75	103.56
18-2b	0.05	0.01	0.56	0.68	106.98
11-1a	0.05	0.03	0.65	0.72	149.79
11-1b	0.07	0.03	0.64	0.61	157.79
18-3a	0.05	0.11	0.62	0.65	149.33
18-3b	0.10	0.13	0.62	0.59	152.18

minor axis lengths, major and minor axis slopes, perimeter, and shape factor. The definitions of the individual parameters are illustrated in Figure 3 and explained in Table 2.

## RESULTS

### MINERAL COMPOSITION

Feldspar (mainly Na-rich plagioclase and K-feldspar), quartz, and mica (muscovite, biotite, muscovite, and chlorite) are the most common minerals in the samples investigated. Amphibole was observed in only two samples (Samples No. 07-2 and 15-1). Minerals forming very small grains were not quantitatively distinguished, due to the restricted magnification and resolution of the polarising microscope (see column “NI” in Table 3). These minerals, analysed only qualitatively utilizing SEM/EDS, were mostly composed of quartz, feldspar (K-feldspar > plagioclase), and mica (muscovite, biotite, sericite, chlorite). Very fine grained calcite was observed only in sample No. 18-1.

The accessory minerals (< 1.0 vol. %) were investigated employing both polarising microscopy and the SEM/EDS method. The most common were apatite, titanite, ilmenite, rutile, and Fe-oxyhydroxides (forming very small grains (inclusions) of < 0.05 µm diameter). Graphite was observed only in one sample (Sample No. 18-1) dispersed in a fine-grained matrix.

### GRAIN SIZE

The average values of equivalent diameter ( $D_{equiv}$ ) vary between 0.02 and 0.39 mm (Table 4).

Three groups of samples were distinguished, according to the diameter (classification of grain size accepted from Robertson, 1999):

- very fine-grained samples - grain sizes less than 0.032 (Sample No. 18-1);
- fine-grained samples - grain sizes between 0.032 and 0.25 (Samples No. 18-2, 18-3, 11-1, and 04-1);
- medium-grained samples - grain sizes greater than 0.25 (Samples No. 07-2 and 15-1).

The grain size variability (resp. standard mean deviation of equivalent diameter, SMD) enables one to distinguish even-grained samples from uneven-grained ones. Samples with SMD≈0 (Samples No. 18-1, 18-2, and 11-1) are classified as even-grained. Another five samples indicating a high SMD were classified as uneven-grained (Table 4).

### GRAIN SHAPE PARAMETERS

A grain shape was characterised by shape factor (SF) and by grain ellipticity (Table 4). The samples show small difference in SF. The SF of most of the samples varies between 0.5 and 0.6. The highest shape factor was found in connection with samples No. 18-1, 18-2, 18-3 and 11-1 (SF > 0.6).

The average values of grain ellipticity vary between 0.47 - 0.60. Average values reaching 0.7 are less common typical of samples with more elongated grains (e.g. Samples No. 18-1, 18-2 and 11-1).

Different values of SF and grain ellipticity were found between samples parallel and perpendicular to

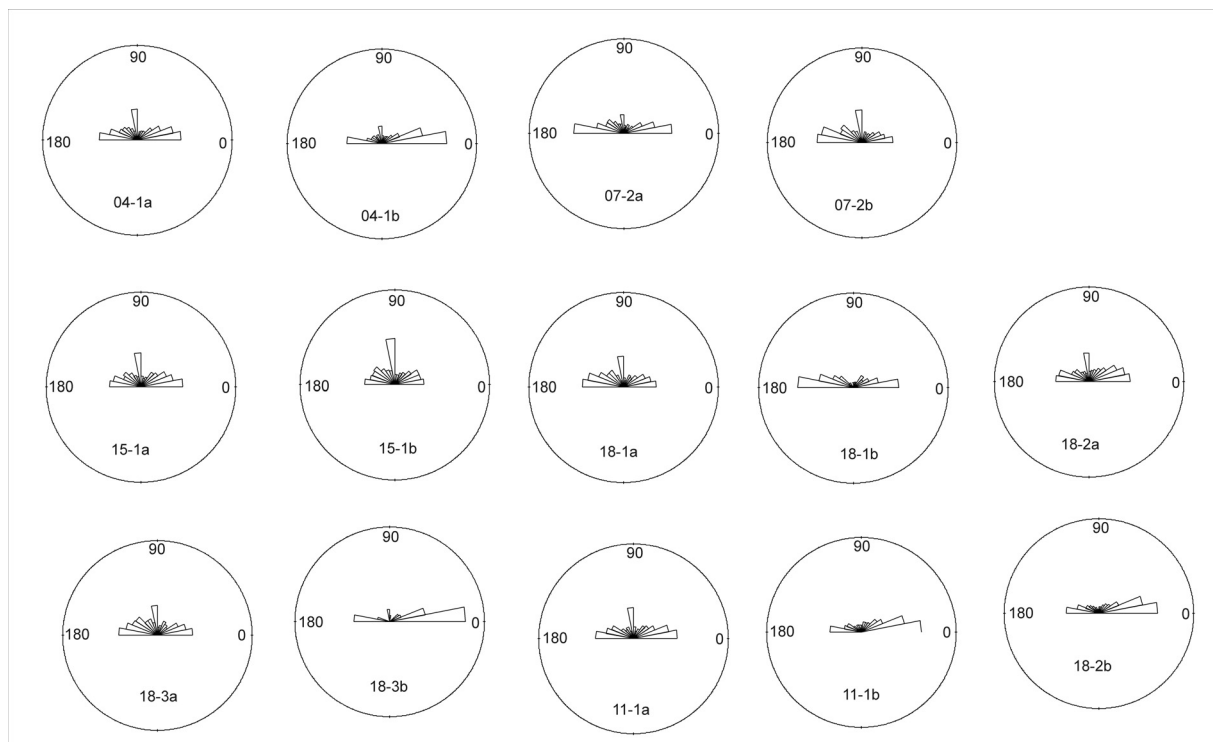


**Fig. 4** Rose diagrams indicating shape preferred orientation.

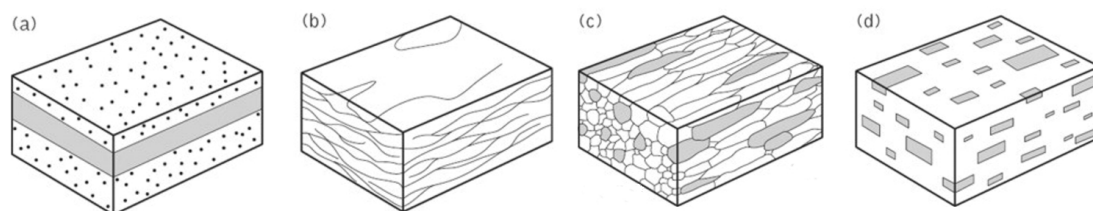


**Fig. 5** Fabric elements that define foliations. In each case the foliation is parallel to the top of the block. (a) compositional banding; (b) parallel discontinuities; (c) elongate mineral grains; (d) inequant mineral grains (accepted from Twiss and Moores, 1992, modified).

the foliation. It is suggested dependence between existence of foliation and mineral arrangement within the rock. Elongated grains are arranged by their longer axis in the same direction which creates rock structure macroscopically observed as foliation (see Figure 5, Part c; Twiss and Moores 1992). Samples (thin sections, t.s."b" in Figure 5) parallel to foliation contain more irregular (resp. more elongated) grains. Samples (thin sections, t.s."a" in Figure 5) perpendicular to foliation contain more circle-like grains.

#### **SHAPE PREFERRED ORIENTATION**

The shape preferred orientation was calculated from the major axis slope, and graphically illustrated using rose diagrams (see Figure 4). Samples No. 18-1, 18-2, 18-3, 11-1, and partially Sample No. 04-1 ("b" samples - parallel to foliation) showed the most intensive shape preferred orientation in the subhorizontal direction of rose diagrams (parallel to the foliation). The shape preferred orientation of the other three samples is less obvious. The strongest shape preferred orientation is obvious with mica

**Table 5** Deformation-recrystallization characteristics (DRC) of quartz. Q-pe - quartz with patchy extinction, Q-ue - quartz with undulose extinction, Q-sb - quartz with serrated boundaries, Q-BLG - quartz with bulging recrystallization, Q-SGR - quartz with subgrain rotation recrystallization, Q-GBM - quartz with grain boundary migration recrystallization.

Sample No.	DRC of quartz	Sample No.	DRC of quartz
04-1a	Q-pe, Q-GBM	18-2a	Q-BLG, Q-SGR
04-1b	Q-pe, Q-GBM	18-2b	Q-BLG, Q-SGR
07-2a	Q-ue, Q-GBM	11-1a	Q-pe, Q-sb
07-2b	Q-ue, Q-GBM	11-1b	Q-pe, Q-sb
15-1a	Q-GBM, Q-sb	18-3a	Q-BLG, Q-SGR
15-1b	Q-GBM, Q-sb	18-3b	Q-BLG, Q-SGR
18-1a	Q-sb, Q-BLG		
18-1b	Q-sb, Q-BLG		

grains, due to their flaky habitus. Less visible is the shape preferred orientation of quartz and feldspar, which is mainly caused by an allotriomorphic habitus (in the case of quartz), and alteration (sericitisation of feldspars).

#### **SPECIFIC SURFACE**

A high specific surface indicates a high number of boundaries between the individual grains. The highest specific surface values were calculated for Samples No. 18-1, 18-2, 18-3, and 11-1 (see Table 4). These samples are characterised by very small grain size (equivalent diameter varying between 0.01 and 0.05 mm), which essentially increases the specific surface. The second group of samples (Samples No. 04-1, 07-2, and 15-1) show a specific surface three to five times lower (mainly affected by increasing grain sizes from 0.24 to 0.39 mm).

#### **STRUCTURAL AND MINERAL INHOMOGENEITIES**

Veins and porphyric clasts are very rare components, representing structural and mineral inhomogeneities in the investigated samples. The veins (see Figure 6, Part A, B) were observed cutting some gneiss samples (Samples No. 15-1, and 18-2) in a direction perpendicular (or almost perpendicular) to the rock foliation. They are, at maximum, 50 to 100  $\mu\text{m}$  wide and mainly composed of calcite and chlorite. Some calcite veins were found to be surrounded by rims rich in Fe-oxyhydroxides and sericite.

Porphyric clasts, observed in phyllite (Sample No. 18-1) and gneiss (Sample No. 18-2), are mainly composed of quartz (resp. quartz-feldspar) aggregate (see Figure 6, Part C, D). The equivalent diameter of the porphyric clasts exceeds 20 $\times$  to 100 $\times$  the average diameter of the samples. The shape preferred

orientation of the porphyric clasts does not correlate with the foliation or the shape preferred orientation of the complete sample.

#### **DEFORMATION AND RECRYSTALLIZATION CHARACTERISTICS OF QUARTZ**

Special attention was paid to the deformation and recrystallization characteristics (DRC) of quartz in the investigated samples. The DRC were classified according to Drury and Urai (1990), Hirth and Tullis (1992), and Stipp et al. (2002).

Six different types of quartz were distinguished in the aggregates with respect to their microstructure, deformation, and recrystallization: quartz with undulose extinction (Q-ue), quartz with patchy extinction (Q-pe), quartz with serrated boundaries (Q-sb), quartz with bulging recrystallization (Q-BLG), quartz with subgrain rotation recrystallization (Q-SGR), and quartz with grain boundary migration recrystallization (Q-GBM) (see Table 5 and Figure 7). Quartz with patchy extinction, serrated boundaries, and/or quartz recrystallized by the bulging recrystallization mechanism are typical of low-temperature conditions. Quartz recrystallized by the subgrain rotation mechanism is typical of medium temperature conditions, and quartz recrystallized by the grain boundary migration mechanism is typical of high temperature conditions (Stipp et al., 2002).

#### **DISCUSSION**

##### **PETROGRAPHIC CHARACTERIZATION OF ROCK TYPES**

Based on the mineral composition and microstructure, the samples were classified as phyllite, orthogneiss, or schist. Phyllite (Sample No. 18-1) was distinguished consistent with very small grain size,

regular (resp. circle-like) grain shape, and significant shape preferred orientation. Graphite indicate its sedimentary origin. The sample can be classified as calcite-rich phyllite based on the high content of calcite in fine-grained matrix. Schists (Samples No. 11-1 and 18-3) are strongly foliated, fine grained, containing weakly elongated grains. Low to medium temperature conditions of metamorphism are indicated by the deformation and recrystallization characteristics of quartz, and by significant amounts of sericite, muscovite, and/or biotite. The sedimentary origin and later metamorphism of both phyllite and schists samples has been confirmed by previous structural and tectonic studies (e.g., Šitavanc and Souček, 1986; Novák et al., 1988).

Orthogneisses (Samples No. 04-1, 07-2, and 15-1) show fine to medium grain sizes, with more elongated shapes of the individual grains. The shape preferred orientation is less visible. Plagioclase is more common than K-feldspar. Medium to high temperature conditions affecting orthogneisses are indicated by grain boundary migration recrystallization, visible in quartz grains and by the presence of biotite and/or amphibole. The origin of orthogneisses was explained by the metamorphism of granitic rock types (e.g., Puda and Urbánek, 1972; Lundqvist, 1979).

More complicated is the characterisation of the last sample (Sample No. 18-2, indicated in the literature as “hybrid gneiss”, Zimák and Novotný, 2000). Some modern studies explain the rock as orthogneiss derived from plutonic rock types (Zimák and Novotný, 2000). In contrast, a possible sedimentary source of the rock has been confirmed by geochemical studies (Novák et al., 1988). Based on its microscopic characterisation, the sample shows parameters similar to those of schists or phyllite: fine grained, foliated with more isometric grain shape, containing muscovite, sericite biotite, as well as quartz; indicating a low to medium recrystallization mechanism.

#### **POSSIBLE APPLICATION OF ROCK MICROSTRUCTURE PARAMETERS**

The occurrence, degree, and mean direction of a shape preferred orientation of elongated particles (“shape-fabric”) has been accepted to be a primary indicator of the paleocurrents and flow rheology assessments (Capaccioni et al., 1997). Quartz microstructures indicate the thermal history of rocks (e.g., Stipp et al. 2002). Porphyric clasts and their spatial relationship with the surrounded rock are important kinematic indicators in fine grained metamorphic rocks (e.g., Passchier and Speck, 1994). Microcracks and veins indicate young tectonic movements of the rocks, as well as the circulation of fluids (e.g., Kreuzer, 2004; Caine et al., 2010).

Structural and mineral inhomogeneities indicate possible tectonic movements in the Silesian domain (Samples No. 15-1, 18-1, 18-2 and 18-3). In the same

area, the indicators of tectonic movements were found by GPS epoch measurements (Schenk et al., 2003, 2010a, 2010b). Final application of both structural and mineral inhomogeneities in the interpretation of the kinematic history of the Silesian domain have not yet been completed, due to the restricted number of sampling points and low number of investigated samples. Suggested further research includes: (1) selection of new sampling points indicating the kinematic history on the macro scale; (2) selection of more sampling points situated closer to each other; and (3) the sampling of a higher number of samples for investigation from each point.

#### **CONCLUSIONS**

Orthogneiss, schists, and phyllite were distinguished according to their mineral composition and microstructure parameters. Orthogneisses are coarser, with weaker foliation and an irregular grain shape. Schists are fine grained, with strong foliation and a circle-like grain shape. The igneous (resp. sedimentary) origin of orthogneisses (resp. schists) was verified from a study of the literature. Schists were found to be affected by low to medium metamorphic conditions, based on the mineral assemblages and microscopic characteristics of the quartz. In contrast, the orthogneisses investigated were mostly affected by a medium to high degree of metamorphism. Those samples designated as “hybrid gneiss” in the literature showed microstructure parameters similar to schists. The application of petrographic image analysis enabled us to quantify such parameters as mineral composition, shape preferred orientation, grain size, and grain shape.

#### **ACKNOWLEDGEMENTS**

This study was undertaken as a part of the projects: “Alkali-silica reaction of crushed aggregates in mortar specimens” (Project No. 103/09/P139, supported by the Czech Science Foundation) and the program of Center of Earth’s Dynamics Research (project LC506, supported by the Ministry of Education, Youth and Sports of the Czech Republic). Also it is acknowledged the financing which came from the Swedish Transport Administration (Project: “Establishment of data base for mechanical characteristics of the common rock materials used for aggregate production. The work corresponded to the Research Plans No. MSM0021620855 and AVOZ30460519. We are grateful to Diotech, Ltd. (for the preparation of polished thin sections) to M. Racek (for assistance with the SEM/EDS).

#### **REFERENCES**

- del Amo, D.G. and Perez, B.C.: 2001, Diagnosis of the alkali-silica reactivity potential by means of digital image analysis of aggregate thin sections, *Cem. Concr. Res.*, 31, 10, 1449–1454.
- Bucher, K. and Frey, M.: 1994, *Petrogenesis of metamorphic rocks*. Springer, Berlin, 318pp.

- Caine, J.S., Bruhn, R.L. and Forster, C.B.: 2010, Internal structure, fault rocks, and inferences regarding deformation, fluid flow, and mineralization in the seismogenic Stillwater normal fault, Dixie Valley, Nevada, *J. Struct. Geol.*, In Press.
- Capaccioni, B., Valentini, L., Rocchi, M.B.L., Nappi, G. and Sarocchi D.: 1997, Image analysis and circular statistics for shape-fabric analysis: applications to lithified ignimbrites. *Bull. Volc.*, 58, 501–514.
- Claesson, S. and Lundqvist, T.: 1995, Origins and ages of Proterozoic granitoids in the Bothnian Basin, central Sweden; isotopic and geochemical constraints, *Lithos*, 36, 2, 115–140.
- Drury, M.R. and Urai, J.L.: 1990, Deformation-related recrystallization processes, *Tectonophys.*, 172, 235–253.
- Ehrlich, R., Crabtree, S.J., Horkowitz, K.O. and Horkowitz, J.P.: 1991, Petrography and Reservoir Physics: I, II and III, *Am. Assoc. Petrol. Geol. Bull.*, 75, 1547–1562.
- Heilbronner, R.: 2000, Automatic grain boundary detection and grain size analysis using polarization micrographs or orientation images, *J. Struct. Geol.*, 22, 969–981.
- Hirth, G. and Tullis, L.: 1992, Dislocation creep regimes in quartz aggregates, *J. Struct. Geol.*, 14, 145–159.
- Howarth, D.F. and Rowlands, J.C.: 1987, Quantitative assessment of rock texture and correlation with drillability and strength properties, *R. Mech. R. Eng.*, 20, 57–85.
- Kreuzer, O.P.: 2004, How to resolve the controls on mesothermal vein systems in a goldfield characterized by sparse kinematic information and fault reactivation—a structural and graphical approach, *J. Struct. Geol.*, 26, 6–7, 1043–1065.
- Kryza, R. and Pin, C.: 2010, The Central-Sudetic ophiolites (SW Poland): Petrogenetic issues, geochronology and palaeotectonic implications, *Gondwana Res.*, 17, 2-3, 292–305.
- Le Maitre, R.W. (Ed.): 1989, A classification of igneous rocks and glossary of terms. Recommendations of the IUGS subcommission of the systematics of igneous rocks, Blackwell, Oxford, 193pp.
- Lukschová, Š., Příklad, R. and Pertold, Z.: 2009, Petrographic identification of alkali-silica reactive aggregates in concrete from 20th century bridges, *Constr. Build. Mat.*, 23, 2, 734–741.
- Lundqvist, T.: 1979, The Precambrian of Sweden, *Sveriges Geologiska Undersökning CNR768*, 73, 9, 87pp.
- McPhie, J., Doyle, M. and Allen, R.: 1993, Volcanic textures: a guide to the interpretation of textures in volcanic rocks, University of Tasmania, ISBN 085901522X, 190pp.
- Mason, R.: 1990, Petrology of the metamorphic rocks, Unwin Hyman Ltd., London, UK, 230pp.
- Novák, M., Sidorinová, T. and Souček, J.: 1988, Petrologic research of Jeseník area (Petrologický výzkum v jesenícké oblasti, in Czech), unpublished report, GFP062161, 133pp.
- Ondra, P. and Potměšil, O.: 1965, Final report about geologic mapping of Javorník area in the scale of 1:100000 (Závěrečná zpráva o geologickém mapování Javornického výběžku v měřítku 1:10000, in Czech), unpublished technical report, GFP017015, 86pp (+6app.).
- Passchier, C.W. and Speck, P.J.H.R.: 1994, The kinematic interpretation of obliquely-transected porphyroblasts: an example from the Trois Seigneurs Massif, France, *J. Struct. Geol.*, 16, 7, 971–984.
- Petruk, W.: 1986, Image analysis: an overview of developments. CAMNET Report 86-4E, 5pp.
- Puda, S. and Urbánek, J.: 1972, Final report about field prospection of aggregates (Závěrečná zpráva z vyhledávacího průzkumu kamene, in Czech), unpublished technical report, GFP023552, 105pp (+64app.).
- Příklad, R.: 2006, Assessment of rock geomechanical quality by quantitative rock fabric coefficients: Limitations and possible source of misinterpretations, *Eng. Geo.*, 87, 3–4, 149–162.
- Robertson, S.: 1999, BGS Rock Classification Scheme, Volume 2, Classification of Metamorphic Rocks, British Geological Survey, Research Report RR 99-02, British Geological Survey, UK, 26pp.
- Rutland, R.W.R., Kero, L., Nilsson, G. and Stølen, L.K.: 2001, Nature of a major tectonic discontinuity in the Svecofennian province of northern Sweden, *Precambrian Res.*, 112, 3–4, 211–237.
- Sandström, B., Tullborg, E.-L., Larson, S.Å. and Page, L.: 2009, Brittle tectonothermal evolution in the Forsmark area, central Fennoscandian Shield, recorded by paragenesis, orientation and <sup>40</sup>Ar/<sup>39</sup>Ar geochronology of fracture minerals, *Tectonophys.*, 478, 3-4, 158–174.
- Schenk, V., Schenková, Z., Cacoň, S., Kontny, B., Bosa, J. and Kottbauer, P.: 2003, To geodynamic interpretations of GPS data monitored on the EAST SUDETEN network. *Acta Montana, Ser. A*, 24, 131, 87–97.
- Schenk, V., Schenková, Z., Cajthamlová, M. and Fučík, Z.: 2010a, GEONAS – Geodynamic network of permanent GNSS stations within the Czech Republic. *Acta Geodyn. Geomater.*, 7, 1, 99–111.
- Schenk, V., Schenková, Z., Bosa, J. and Kontny, B.: 2010b, Reliability of GPS data for geodynamic studies. Case study: Sudeten area, the Bohemian Massif. *Acta Geodyn. Geomater.*, 7, 1, 113–128.
- Siegesmund, S., Helming, K. and Kruse, R.: 1994, Complete texture analysis of a deformed amphibole - comparison between neutron diffraction and U-stage data, *J. Struct. Geol.*, 16, 1, 131–142.
- Spry, A.: 1969, Metamorphic textures, Pergamon, London, 350pp.
- Stipp, M., Stünitz, H., Heilbronner, R. and Schmidt, S.M.: 2002, The eastern Tonale fault zone: a "natural laboratory" for crystal plastic deformation of quartz over a temperature range from 250 to 700° C, *J. Struct. Geol.*, 24, 1861–1884.
- Svoboda, J., Baneš, K., Dudek, A., Holubec, J., Chaloupský, J., Kodým, O., Malkovský, M., Odehnal, L., Polák, A., Poubá, Z., Satran, V., Škvor, V. and Weiss, J.: 1964, Regional geology of ČSSR (Regionální geologie ČSSR, in Czech), part. 1. ÚÚG ČSAV, Prague, 377pp.
- Systat Software Inc., SigmaScan Pro 5.0.0, <http://www.sigmaplot.com/index.php> (24-08-2010)
- Šitavanc, D. and Souček, J.: 1986, Geochemistry of rocks from Keprník nape (Geochemie hornin keprnické klenby, in Czech), unpublished report, GFP055275, 55pp.

- Štípská, P., Schulmann, K., Thompson, A.B., Ježek, J. and Kröner, A.: 2001, Thermo-mechanical role of a Cambro-Ordovician paleorift during the Variscan collision: the NE margin of the Bohemian Massif, *Tectonophys.*, 332, 1–2, 239–253.
- Trčková, J., Šrein, V., Šťastný, M. and Živor, R.: 2008, The relationship between gneisses from the Kola superdeep borehole and their surface analogues, *Acta Geodyn. Geomat.*, 5, 1, 57–63.
- Twiss, R. J. and Moores, E. M.: 1992, *Structural geology*, W. H. Freeman, New York, 532pp.
- Vernon, R.H.: 2004, *A practical guide to rock microstructure*, Cambridge University Press, 650pp.
- Zhang, B.L., Lin, C.Y. and Shi, L.B.: 2002, Microstructural features of fault gouges from Tianjingshan-Xiangshan fault zone and their geological implications, *Sci. China Ser. D - Earth Sci.*, 45, 1, 72–80.
- Zimák, J. and Novotný, P.: 2000, Minerals of Alpine paragenesis in aplite, Bohutín quarry, Šumperk (Nerosty puklinové asociace v žilách aplitu v lomu Zbová u Bohutína, okres Šumperk, in Czech), *Bull. Min. Pet. Dep. Nat. Mus.*, 8, 253–259.

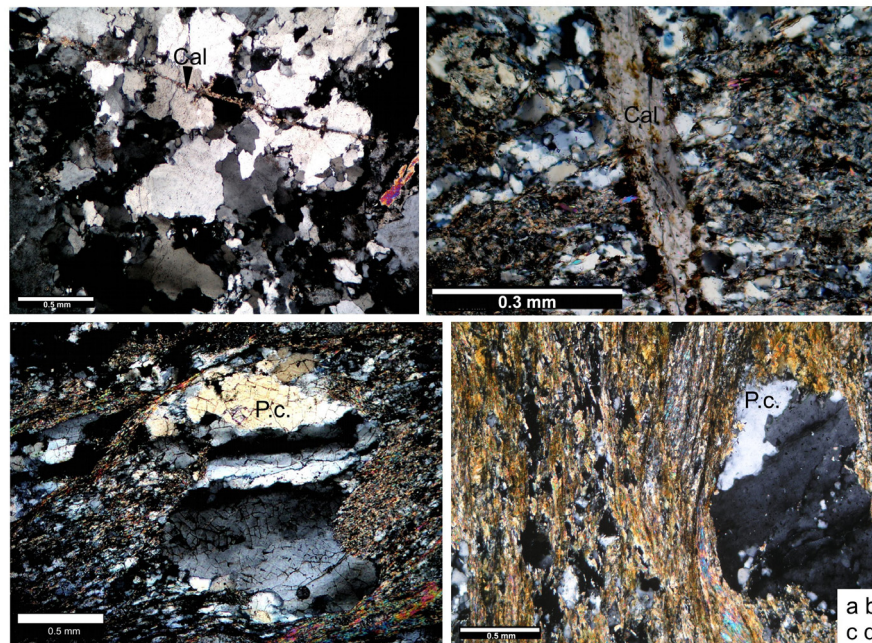


**Fig. 6** Calcite filled veins (cal, parts a, b) and porphyritic clasts (P.c., parts c, d) observed in orthogneiss (part a, sample No 15-1), “hybrid” gneiss (parts b, c, sample No. 18-2) and phyllite (part d, sample No. 18-1). Polarising microscope, crossed nicols.

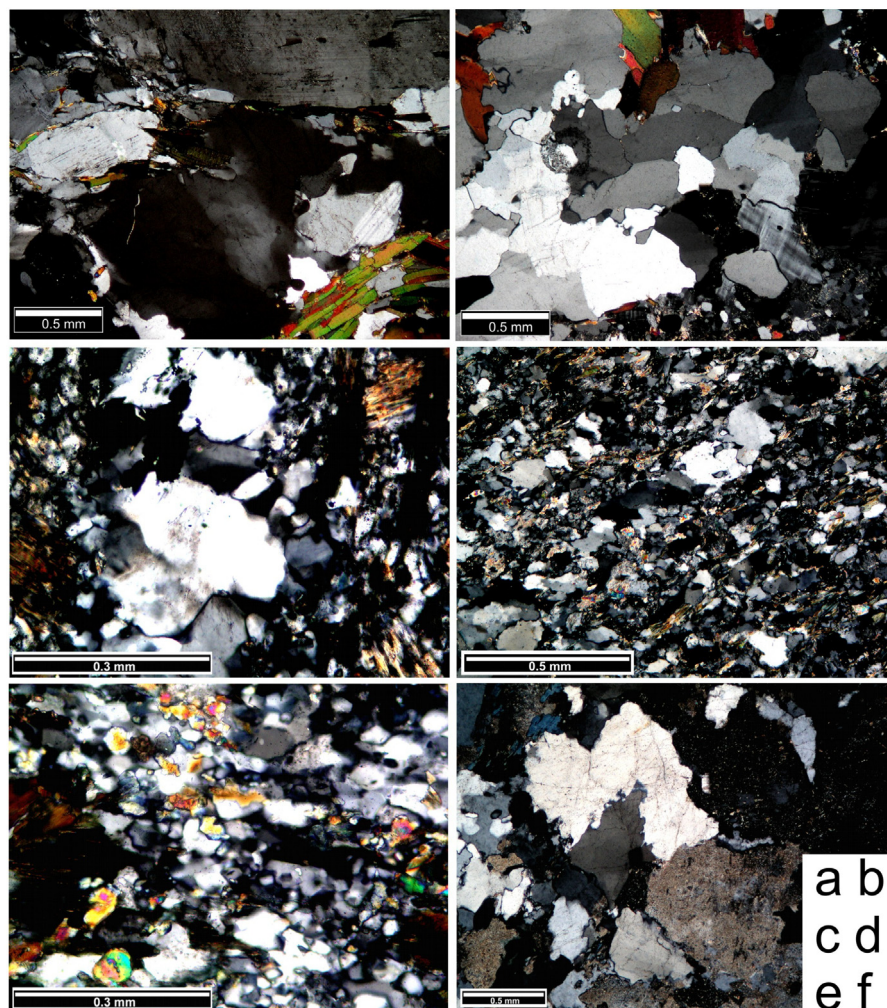


**Fig. 7** Deformation and recrystallization characteristics of quartz-rich aggregates – quartz with patchy extinction and grain boundary migration recrystallization (a), quartz with grain boundary migration recrystallization (b), quartz with bulging-to-subgrain rotation recrystallization mechanism (c), quartz with serrated boundaries and bulging recrystallization mechanism (d, e), and quartz with grain boundary migration recrystallization and serrated boundaries (f). Polarising microscope, crossed nicols. Samples No. 04-1a (a), 07-2a (b), 11-1a (c), 18-2a (d), 18-3b (e) and 15-1a (f).